Nano Energy (2014) 8, 196–204

Available online at www.sciencedirect.com

ScienceDirect

journal homepage: www.elsevier.com/locate/nanoenergy

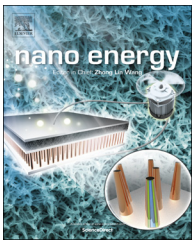

RAPID COMMUNICATION

Heterogeneous branched core-shell SnO_2-PANI nanorod arrays with mechanical integrity and three dimentional electron transport for lithium batteries

Wangwang Xu[1], Kangning Zhao[1], Chaojiang Niu, Lei Zhang, Zhengyang Cai, Chunhua Han, Liang He*, Teng Shen, Mengyu Yan, Longbing Qu, Liqiang Mai*

State Key Laboratory of Advanced Technology for Materials Synthesis and Processing, WUT-Harvard Joint Nano Key Laboratory, Wuhan University of Technology, Wuhan 430070, China

Received 13 March 2014; received in revised form 15 May 2014; accepted 5 June 2014
Available online 18 June 2014

KEYWORDS
Core-shell;
Heterogeneous;
SnO_2 nanorod arrays;
Conducting polymer;
Lithium batteries

Abstract
SnO_2 with high theoretical capacity has long suffered from its instinct large volume variation and low electrical transport linked to poor cycling stability and rate performance. Here we present the heterogeneous branched core-shell SnO_2-PANI nanorod arrays which have been successfully designed and fabricated by an efficient and facile hydrothermal treatment followed by electrodeposition. The heterogeneous core-shell SnO_2-PANI nanorod arrays exhibit a high reversible capacity of 506 mAh/g after 100 cycles, resulting the capacity fading of 0.579% per cycle between 20 and 100 cycles, much lower than that of nanosheet-assembled hierarchal SnO_2-PANI nanorod arrays (1.150%) and bare SnO_2 nanorod arrays (1.151%). At high current density of 3000 mA/g, heterogeneous core-shell SnO_2-PANI nanorod arrays maintain a capacity of 660 mAh/g after the current density returns to 100 mA/g, 3 times as high as that of nanosheet-assembled hierarchal SnO_2-PANI nanorod arrays (206 mAh/g) and 6 times as high as that of bare SnO_2 nanorod (124 mAh/g). The enhanced electrochemical performance can be attributed to the branched conductive PANI shells, which not only release the stress of volume expansion and maintain mechanical integrity during cycling, but also realize three

*Corresponding authors.
E-mail addresses: hel@whut.edu.cn (L. He), mlq518@whut.edu.cn (L. Mai).
[1]These authors contributed equally to this work.

http://dx.doi.org/10.1016/j.nanoen.2014.06.006

dimensional transport for electrons. Our work demonstrates a great potential for the application of heterogeneous branched core-shell PANI-SnO_2 nanorod arrays for lithium batteries.

Introduction

Rechargeable lithium batteries (LIBs) have mainly been employed as energy storage for popular mobile devices such as cellular phones and lap tops [1-4]. Nowadays, their applications have been expanded to a larger scale, particularly electric vehicles (EVs) [5] and plug-in hybrid electric vehicles (PHEVs) [6]. Increasing applications have stimulated higher demand of energy storage electrode materials, such as larger capacity, better rate capability and more safety [7-12].

SnO_2 with a theoretical capacity value (781 mAh/g) twice as high as commercial graphite (372 mAh/g) is considered as one of the most promising candidates for anodes [13]. SnO_2 nanorod arrays (NA) have been intensively studied due to the good contact between the current collector and electrode [14-18]. Significant capacity fading, however, is still a huge obstacle at both long term and high rate cycling due to the frustration and pulverization, by the large volume expansion-contraction (~300%) during battery cycling, and kinetic limitations of its intrinsic nature [19]. The reaction of tin with lithium to yield $Li_{4.4}Sn$ implies a 440% volume increase in the number of atoms present in each active particle, which brings about a huge volume increase leading a loss of contact between the grains and the current collector [20]. Moreover, slow kinetic of electron transport [14,19,21] resulting from the inefficient one dimensional electron transport is still a huge obstacle for the nanorod arrays, especially for the part of nanorods far from the current collector, during lithiation and delithiation process [22,23].

In order to adapt the huge volume variation and improve the electron transport, conducting polymer [24-29], due to its instinct high conductivity has become an attractive additive for electrode materials to overcome the current issues and challenges. Jeong et al. constructed hierarchical hollow spheres of Fe_2O_3@polyaniline (PANI) demonstrating excellent electrochemical characteristics as an anode for LIBs, such as large reversible capacity, good rate capability, and long-term cycling stability [30]. Moreover, construction of core-shell structure can offer great advantages, such as

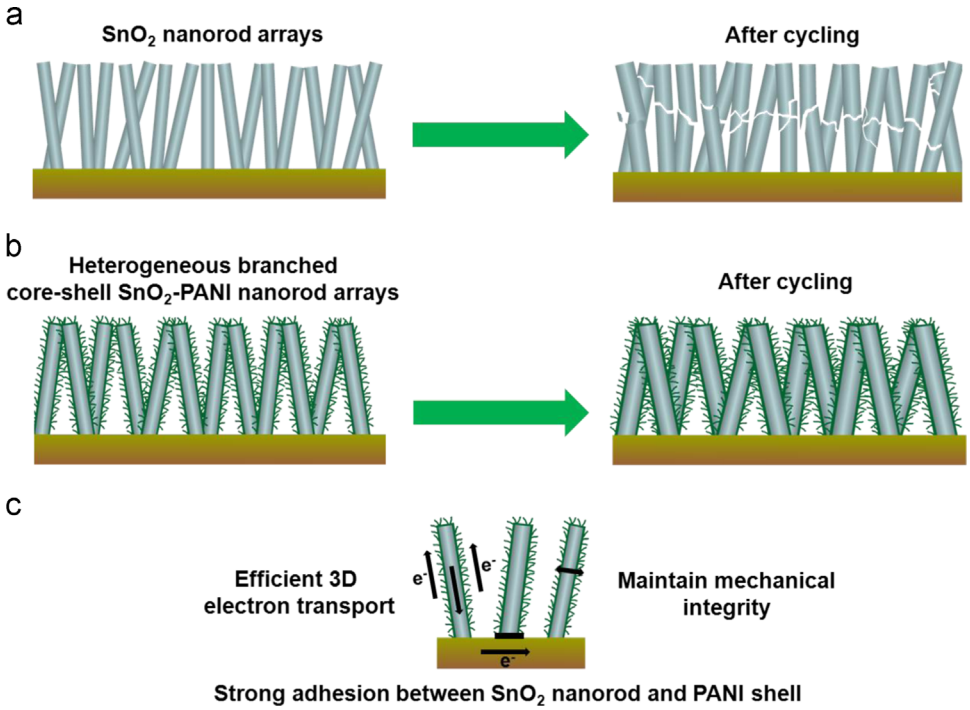

Figure 1 Schematic illustrations of heterogeneous branched core-shell SnO_2-PANI nanorod arrays during cycling. (a) The structural degradation of SnO_2 nanorod arrays during cycling. SnO_2 nanorods tend to pulverize. Much of the material loses contact with the current collector, resulting in poor transport of electrons; (b) Due to SnO_2 nanorods coated by PANI shells, they do not pulverize or break into smaller particles during cycling. Moreover, facile strain relaxation in the PANI allows them to increase in diameter and length without pulverization. (c) The conducting polymer coating nanorod arrays offer efficient 3D electron transport and strong adhesion between nanorod and PANI shell, maintaining mechanical integrity of nanorod during cycling.

good protection of the core, better electron conductivity [31–34]. Wang et al. have designed the Pt–Co nanocatalysts composed of ordered Pt_3Co intermetallic cores with a 2–3 atomic-layer-thick platinum shell showing high activity and stability attributing to the Pt-rich shell and the stable intermetallic Pt_3Co core arrangement [35].

Herein, to combine all these merits and improve the electrochemical performance of SnO_2, we rationally design and prepare the heterogeneous branched core–shell SnO_2–PANI nanorod arrays through a facile and scalable hydrothermal method to obtain SnO_2 nanorod arrays on nickel foam, followed by electrodepositing PANI. The PANI shells are directly grown on SnO_2 nanorods, forming core–shell structure, which ensures mechanical integrity and electric connection between SnO_2 nanorods and nickel foam, meanwhile, realizing binder-free. The PANI shells may serve as the protecting shells for the SnO_2 nanorods to accommodate the dramatic and drastic volume variations, alleviate disintegration and pulverization during lithiation and delithiation. Moreover, both of the highly conductive PANI shells and nickel foam can offer the 3D continuous electron transport for the SnO_2 nanorods. Through coating conducting polymer, heterogeneous branched core–shell SnO_2–PANI nanorod arrays can combine the merits of good contact and efficient diffusion distances for three dimensional (3D) electron transports leading to fast reaction kinetics with fast switching speed (Figure 1). And the core–shell structure can offer good protection of the SnO_2 nanorod core by the PANI shell, ensuring the excellent structure stability. Thus, enhanced rate capability and cyclability of heterogeneous branched core–shell SnO_2–PANI nanorod arrays can be anticipated. To our knowledge, this strategy may be the first report on heterogeneous branched core–shell SnO_2-PANI nanorod arrays.

Material and methods

Synthesis of bare SnO_2 nanorod arrays

In a typical experiment, $SnCl_4 \cdot 5H_2O$ (0.73 g) and NaOH (1.25 g) were dissolved into 30 mL distilled water. After half an hour of magnetic stirring, 50 mg NH_4F was added into solution. The solution was transferred into a Teflon-lined autoclave (50 mL), in which a piece of cleaned nickel foam substrate was beforehand placed standing against the wall, heated to 200 °C for 24 h. The nickel foam act as substrate for SnO_2 nanorod arrays during hydrothermal process. The as-deposited bare SnO_2 nanorod arrays were rinsed repeatedly with deionized water and dried at 60 °C for 8 h. The mass of a SnO_2 nanorod arrays is about 1.67 mg/cm^2.

Preparation of heterogeneous branched core-shell SnO_2-PANI nanorod arrays

Bare SnO_2 nanorod arrays were obtained as the method mentioned above. Then the SnO_2 nanorod arrays were acted as the backbone for the growth of PANI shell. Electrolyte for electro-polymerization of PANI was obtained by dissolving 0.5 mL aniline into 100 mL of 0.01 M H_2SO_4 solution. The electro-polymerization of PANI was carried out in a three-compartment system, using the bare SnO_2 nanorod arrays electrode as the working electrode, Ag/AgCl as the reference electrode and Pt foil as the counter electrode. The PANI shell was deposited by using a CHI760D electrochemical workstation through a cyclic voltammetry (CV) method at a sweep rate of 30 mV/s between −0.2 and 1.6 V for 5 cycles.

Preparation of nanosheet-assembled hierarchical SnO_2-PANI nanorod arrays

Bare SnO_2 nanorod arrays and electrolyte were prepared as mentioned above. The chronopotentionmetry electrodeposition was carried out in a three-compartment system, which is the same with above except by changing the deposition condition to constant anodic current density of 2.5 mA/cm^2. The nanosheet-assembled hierarchical SnO_2-PANI nanorod arrays were obtained when applying time for 1500 s.

Characterization

The crystallographic information of the obtained products was measured with a X-ray diffraction (XRD) measurement using Cu Kα radiation in a 2θ range from 10° to 80° at room temperature. Field emission scanning electron microscopic (FESEM) images were carried out by JEOL-7100F, transmission electron microscopic (TEM) and high-resolution transmission electron microscopic (HRTEM) images were observed by JEM-2100F. Energy dispersive X-ray spectra (EDS) was recorded by using Oxford EDS IE250. Fourier transformed infrared (FTIR) transmittance spectra was recorded using the 60-SXB IR spectrometer. The electrochemical performance was characterized with coin cells of CR2016 type assembled in a glove-box filled with pure argon gas. Lithium foil was used as the anode, a solution of $LiPF_6$ (1 M) in EC/DEC (1:1 vol/vol) was used as the electrolyte, the as-prepared samples as cathode. Galvanostatic charge/discharge measurement was performed with a multichannel battery testing system (LAND CT2001A), electrochemical impedance spectroscopic (EIS) was measured by an Autolab Potentiostat Galvanostat at room temperature.

Results and discussion

Initially, the morphology is characterized by the SEM technique. As shown in Figure 2a, the bare SnO_2 nanorods are about 100 nm in width and 1 μm in length. During the formation of SnO_2 nanorod arrays, NH_4F plays a critical factor for the formation of SnO_2 nanorod. When no NH_4F is added, the SnO_2 nanorod arrays are few and scattered indicating that less SnO_2 nanorods are grown on the nickel foam. When the amount of NH_4F is increased to twice amount, the SnO_2 nanorod arrays are concentrated indicating that more SnO_2 nanorods are grown (Figure S1). The phenomenon can be attributed to the presence of F^-, which can stimulate the substrates to produce more active sites for nucleation [36,37]. The nanosheet-assembled hierarchal SnO_2–PANI nanorod arrays are assembled by the PANI shells which directly grow on the surface of the SnO_2 nanorods (Figure 2b). As for heterogeneous branched core–shell SnO_2–PANI nanorod arrays, the PANI shells coat on the surface of the SnO_2 nanorod arrays forming core–shell structure with

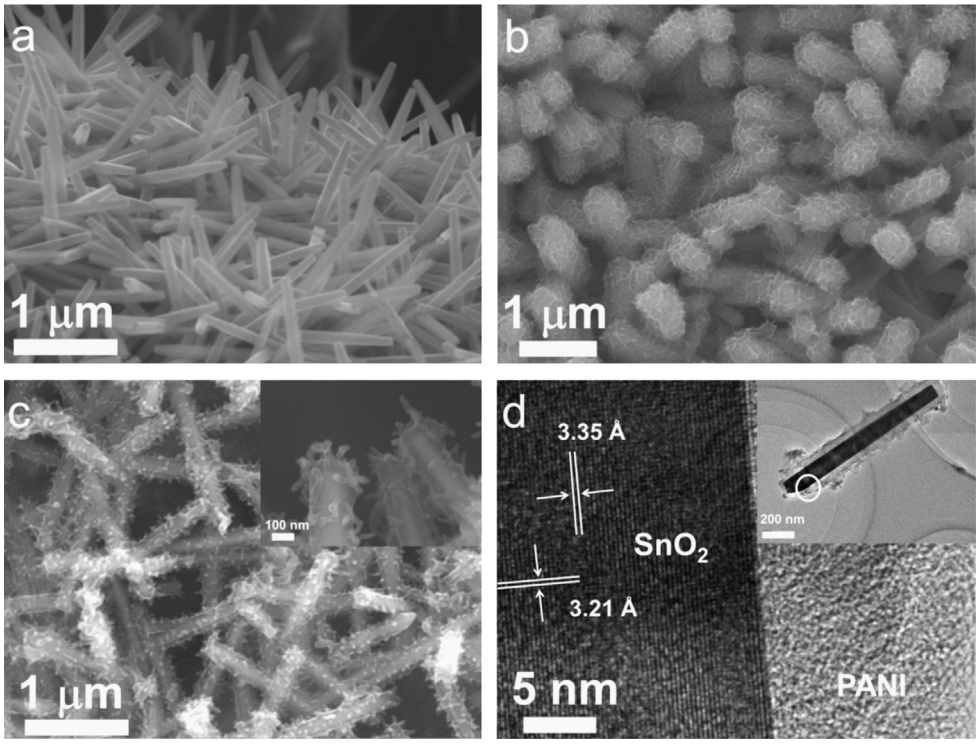

Figure 2 SEM images of (a) bare SnO_2 nanorod arrays, (b) nanosheet-assembled hierarchical SnO_2-PANI nanorod arrays, (c) heterogeneous branched core-shell SnO_2@PANI nanorod arrays (magnified SEM image in inset); (d) HRTEM image of heterogeneous branched core-shell SnO_2-PANI nanorod arrays (TEM image in inset).

branches on the shell. After electrodepositing for 3 cycles, the conducting polymer, coating on the rods, is very smooth (Figure S2). As shown in the magnified SEM image, some small particles are observed on the shells. As the electrodeposition time is increased, the conducting polymer grows on the PANI shells, forming branches (Figure 2c) resulting the heterogeneous branched core-shell structure. As shown in the TEM image (Figure 2d), the conducting polymer, about 20 nm in thickness, is amorphous because no lattice fringe is observed. HRTEM image (Figure 2d) displays a lattice fringe with d-spacing of 0.335 and 0.321 nm, corresponding to the (101) and (001) planes of tetragonal SnO_2 crystal, indicating that mesocrystalline SnO_2 nanorod arrays grow on the nickel foam, with (001)-oriented with four (101) lateral facets [17].

The crystal structure of the three nanorod arrays is determined by XRD. The patterns (Figure 3a) are identified as tetragonal SnO_2 with the lattice parameters of a= 4.7421 Å, b=4.7421 Å, c=3.1901 Å, P42/mnm space group, which match well with those of standard XRD patterns of tetragonal rutile SnO_2 (JCPDF card no. 01-77-0450). No specific peak of PANI is observed, indicating SnO_2 nanorod witness no crystal structure change during electrochemical deposition. In order to identify the polymerization, FTIR is carried out (Figure 3b). For the bare SnO_2 nanorod arrays, only two peaks are observed, 3500 cm^{-1} corresponding to the H-O bond owning to the moisture absorption of KBr powder, 600 cm^{-1} attributing to Sn-O-Sn bond. Both of the SnO_2-PANI nanorod arrays show 5 more peaks, when compared with the bare SnO_2 nanorod arrays. These 5 peaks are, namely, 3400 cm^{-1} attributing to the stretching vibration N-H of an aromatic amine as well as the stretching vibration of absorbed water, 1578 and 1487 cm^{-1} due to the C=C stretching vibrations of quinoid (Q) ring and benzenoid ring, 1306 cm^{-1} belonging to the C−N stretching mode of an aromatic amine, 1130 cm^{-1} which indicates the typical N=Q=N stretching band of PANI [38,39]. Moreover, the existence of PANI shells is clearly proved by the element mappings (Figure 3c) of Sn, O, N, and C elements from the selected area. The outer layer of the SnO_2 nanorods consists of O, N, and C elements, which corresponds with the element of PANI shell, respectively. An EDS line scan (inset of Figure 3c) further confirms that PANI shell coats on the surface of the SnO_2 nanorod. All these prove that the PANI acts as a shell coating on the SnO_2 nanorods. Thus, enhanced rate capability and cyclability of heterogeneous branched core-shell SnO_2-PANI nanorod arrays and nanosheet-assembled hierarchal SnO_2-PANI nanorod arrays can be anticipated.

Further, in order to identify the electrochemical performance of as-prepared samples, coin cells of heterogeneous branched core-shell SnO_2-PANI nanorod arrays, nanosheet-assembled hierarchal SnO_2-PANI nanorod arrays and the bare SnO_2 nanorods are assembled to investigate the electrochemical performance in the voltage range of 0.005-2 V (versus Li^+/Li). The PANI shells contribute a capacity of 20 mAh/g (Figure S3), which can be ignored compared with the high capacity of SnO_2. Generally, the electrochemical reaction of SnO_2 with lithium can be explained as the following two equations [40]:

$$SnO_2 + Li = Li_2O + Sn \quad (1)$$

$$Sn + xLi^+ + e^- = Li_xSn \quad (2)$$

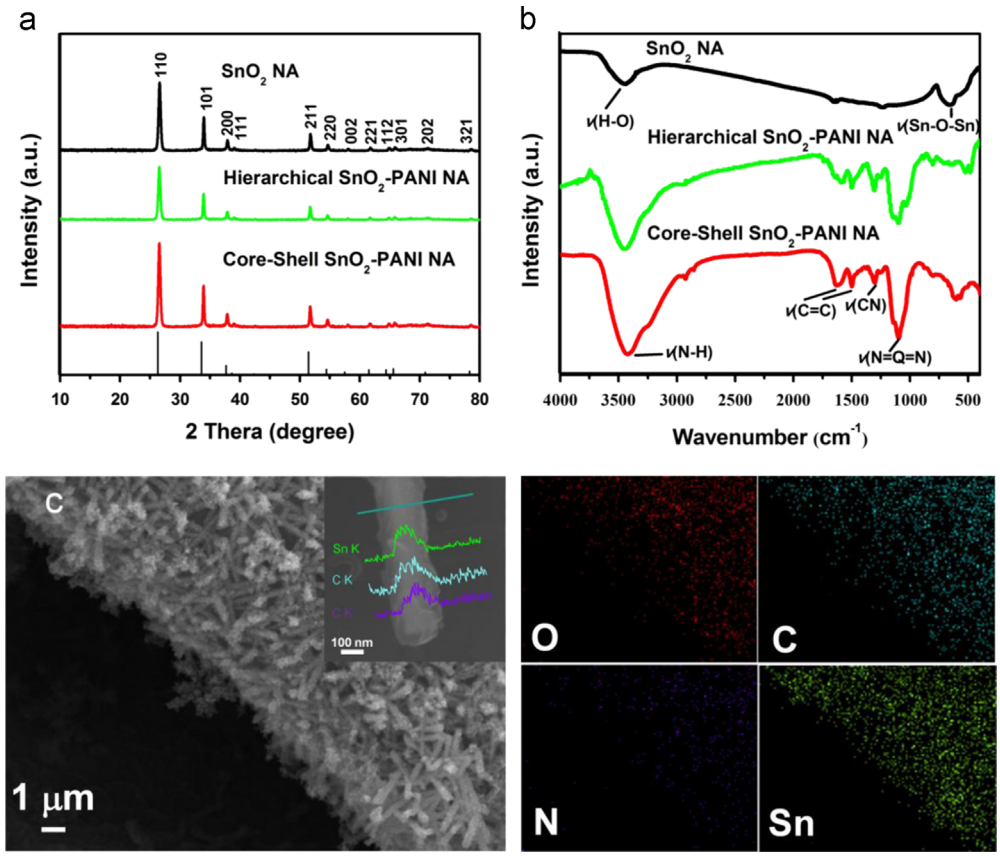

Figure 3 (a) XRD patterns of bare SnO_2 nanorod arrays (noted as SnO_2 NA), heterogeneous branched core-shell SnO_2-PANI nanorod arrays (noted as core-shell SnO_2-PANI NA) and nanosheet-assembled hierarchal SnO_2-PANI nanorod arrays (noted as hierarchal SnO_2-PANI NA); (b) FTIR spectra of bare SnO_2 nanorod arrays, heterogeneous branched core-shell SnO_2-PANI nanorod arrays and nanosheet-assembled hierarchal SnO_2-PANI nanorod arrays; (c) SEM image and EDS mappings of O, N, C and Sn elements (SEM image and corresponding EDS line scan of heterogeneous branched core-shell SnO_2-PANI nanorod arrays, showing the scanning route (white line), the element distribution of tin (green line), carbon (blue line) and nitrogen (purple line) respectively in inset).

Reaction (1) is generally regarded partially reversible. Thus, the theoretical capacity of SnO_2 is determined as 782 mAh/g by the reversible reaction (2). When the current density is 200 mA/g (Figure 4a), the initial discharge capacity of the heterogeneous branched core-shell SnO_2-PANI nanorod arrays is as high as 1715 mAh/g. As for all of the three samples, very rapid capacity decaying is observed during the first 40th cycle. This is mainly due to the irreversible reaction of reaction (1), and the pulverization and disintegration of SnO_2 nanorods. After 100 cycles, the heterogeneous branched core-shell SnO_2-PANI nanorod arrays exhibit 506 mAh/g, showing very stable electrochemical performance. On the contrast, rapid capacity fading is observed for nanosheet-assembled hierarchal SnO_2-PANI nanorod arrays and bare SnO_2 nanorod arrays after 40 and 60 cycles, respectively. This is proved by the *ex-situ* SEM images and TEM images (Figures S4,5). The SnO_2 nanorods were pulverized and broken into small particles. This may results from the expansion and contraction of the SnO_2 nanorods falling down from the nickel foam into the insulated electrolyte. After 100 cycles of nanosheet-assembled hierarchal SnO_2-PANI nanorod arrays, there is little PANI left coating on the surface, as proved by the EDS mapping (Figure S6). The hierarchical PANI shells fall off the SnO_2 nanorods and no protection is preserved. In order to further convince the hypothesis, nanosheet-assembled hierarchical SnO_2-PEDOT nanorod arrays are also synthesized (Figures S8-11) and after 50 cycles, the capacity still witness fast decaying. This may attribute to the weak adhesion between SnO_2 and conducting polymer because the conducting polymer shells are directly grown on the surface of the SnO_2 nanorods. On the contrast, in case of heterogeneous branched core-shell SnO_2-PANI nanorod arrays, the SnO_2 nanorods during cycling were mostly still captured by the PANI shells, instead of disintegrating and pulverizing. After cycling, the SnO_2 nanorods expand about two times, indicating that the PANI shows excellent retractable space for the SnO_2 nanorods to release the stress during cycling.

When the current density is increased to 600 mA/g, enhanced cycle performance is obtained. The heterogeneous branched core-shell SnO_2-PANI nanorod arrays deliver a discharge capacity of 450 mAh/g after 50 cycles, showing a stable performance for the branched core-shell structure compared to the rapid capacity decaying of the nanosheet-assembled hierarchal SnO_2-PANI nanorod arrays and the bare

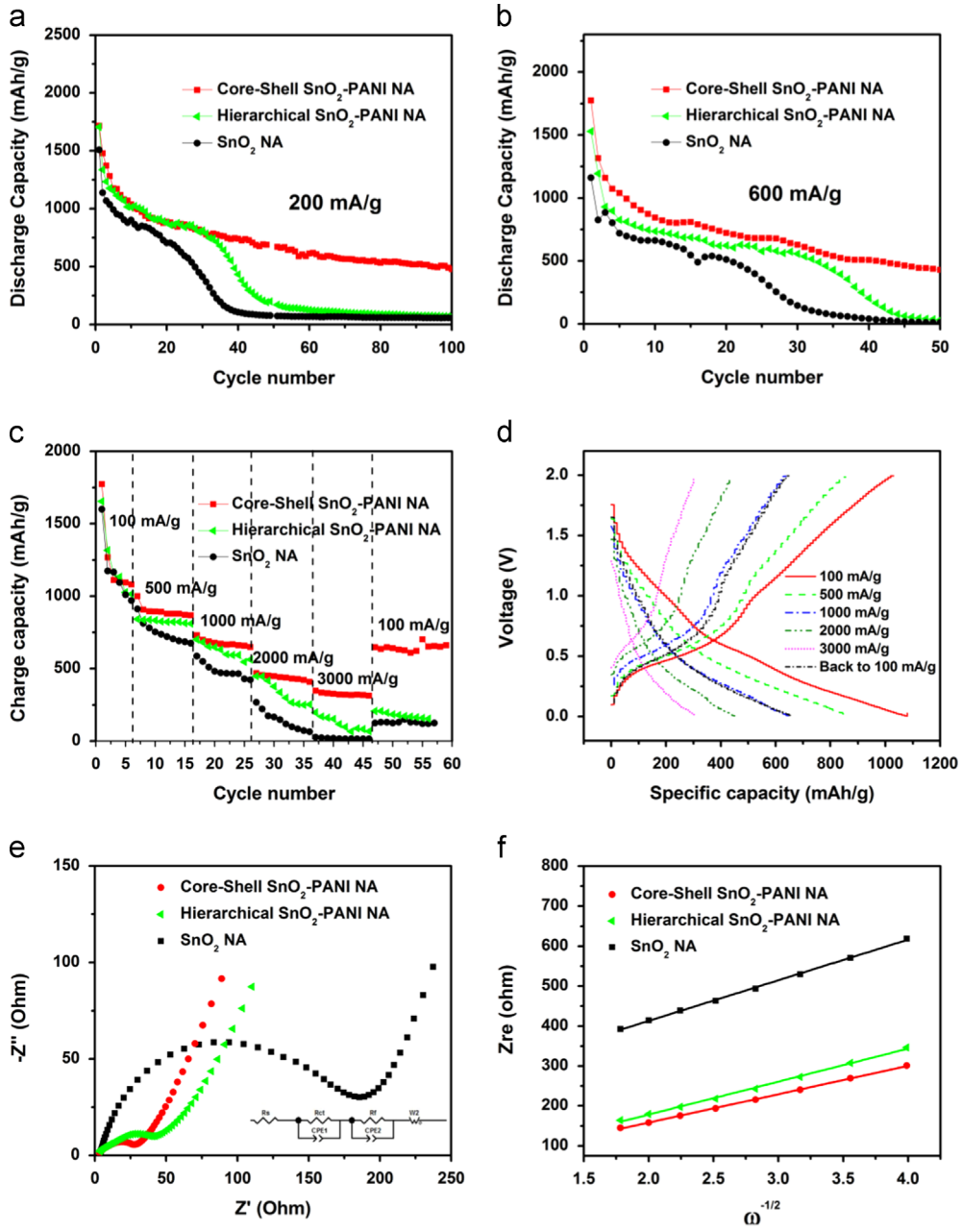

Figure 4 (a, b) Cycling performance of the heterogeneous branched core–shell SnO_2–PANI nanorod arrays at 200 and 600 mA/g, respectively; (c) rate performance at the current density range from 100, 500, 1000, 2000, 3000 and 100 mA/g; (d) charge/discharge profiles of the heterogeneous branched core–shell SnO_2–PANI nanorod arrays at 100, 500, 1000, 2000, 3000 and 100 mA/g corresponding to the rate performance; (e) Nyquist plots of both nanorod arrays electrode at 100% depth of discharge at the 3nd cycle; (f) variations and fittings between Z_{re} and the reciprocal square root of the angular frequency in the low frequency region of heterogeneous branched core–shell SnO_2–PANI nanorod arrays, nanosheet-assembled hierarchal SnO_2–PANI nanorod arrays and bare SnO_2 nanorod arrays.

SnO_2 nanorod arrays (Figure 4b). In order to figure out the difference during cycling, all these three samples after 40 cycles were chosen. As can be observed, bare SnO_2 nanorod arrays and nanosheet-assembled (Figure S5a–c) hierarchical SnO_2–PANI nanorod arrays (Figure S5d–f) are few and scattered and after cycling have disintegrated and pulverized. Moreover, the PANI nanosheets on the nanosheet-assembled hierarchical SnO_2–PANI nanorod arrays have not been observed indicating a loss contact between SnO_2 and PANI shells. However, heterogeneous branched core–shell SnO_2–PANI nanorod arrays (Figure S5g–i) can easily be found on the nickel foam and after cycling were mostly still captured by the PANI shells remaining mechanical integrity, instead of disintegrating and pulverizing. In rate performance test (Figure 4c), it delivers discharge capacities of 1080, 866, 649, 407 and 312 mAh/g at current density of 100, 500, 1000, 2000 and 3000 mA/g, respectively (Figure 4d). The discharge capacity recovers to 660 mAh/g when the current

density goes back to 100 mA/g, showing much better rate performance than those of nanosheet-assembled hierarchal SnO_2-PANI nanorod arrays (206 mAh/g) and bare SnO_2 nanorod arrays (124 mAh/g). With PANI shells forming core-shell structure, the SnO_2 nanorod arrays exhibit enhanced rate capability due to the PANI shells leading good mechanical integrity during fast lithium intercalation and deintercalation. Moreover, the 3D continuous electron transport offering by both the conducting nickel foam and the conducting polymer PANI shell may also be another reason. In this way, fast kinetic of electron transport can be achieved, confirmed by the EIS (Figure 4e). The EIS technology is one of the most powerful tools to study electrochemical reactions, such as the processes occurring at electrode/electrolyte interfaces and Li^+ intercalation/de-intercalation in the interior of cathode/anode materials. In this circuit, R_Ω represents the Ohmic resistance of the electrode system, including the electrolyte and the cell components. R_{ct} represents the charge transfer resistance. CPE and Z_w are the double layer capacitance and the Warburg impedance, respectively [41]. All the Nyquist plots are composed of a depressed semicircle in the medium-frequency region followed by a slanted line in the low-frequency region. The heterogeneous branched core-shell SnO_2-PANI nanorod arrays and nanosheet-assembled hierarchal SnO_2-PANI nanorod arrays both show a much lower resistance of 28 and 48 Ω comparing to the bare SnO_2 nanorods (162 Ω), indicating that the PANI shell indeed enhances the electron transport and modifies the kinetics of the heterogeneous branched core-shell SnO_2-PANI nanorod arrays. Moreover, the values of D were calculated from the inclined lines in the Warburg region using the following equation [41]:

$$D = R^2T^2/2A^2n^4F^4C^2\delta^2 \quad (3)$$

in which T is the absolute temperature, A is the surface area of the cathode electrode, n is the number of electrons per molecule during oxidization, F is the Faraday constant, C is the Li^+ concentration, and δ is the Warburg factor associated with Z_{re} ($Z_{re} \propto \delta\omega^{1/2}$). The Warburg impedance of the heterogeneous branched core-shell SnO_2-PANI nanorod arrays and the nanosheet-assembled hierarchal SnO_2-PANI nanorod arrays are almost equal to that of the bare SnO_2 nanorods demonstrating that the PANI shell does not retard the ion transport.

Based on these results above, an enhanced electrochemical performance of heterogeneous branched core-shell SnO_2-PANI nanorod arrays may be due to the hypothesis below. (1) The core-shell structure offers strong adhesion between SnO_2 nanorods and PANI shells. In this way, the conducting polymer shells protect the inner SnO_2 nanorod and gain excellent structural stability and mechanical integrity leading to enhanced cycling performance. (2) The conducting polymer PANI shell and the highly conducted nickel foam act as the 3D electron transport of the SnO_2 nanorod. Fast electron transport of SnO_2 nanorod can be achieved at the end of rod during cycling, taking advantages of the PANI shell, resulting in the enhanced rate capability.

Conclusions

A simple scalable and controllable approach to synthesize the heterogeneous branched core-shell SnO_2-PANI nanorod arrays is developed by using hydrothermal treatment followed by electrodeposition. Because of their unique composition and architecture, the as-prepared heterogeneous branched core-shell SnO_2-PANI nanorod arrays offer strong adhesion between the nanorod core and the conducting polymer shell, leading to excellent structural stability and mechanical integrity, and also realize 3D electron transport and fast kinetics. Thus, the cycling performance is prolonged and the rate capability is greatly enhanced. This kind of organic and inorganic branched core-shell structure and the effective strategy can be further applied to the high-performance energy storage devices.

Acknowledgments

This work was supported by the National Basic Research Program of China (2013CB934103, 2012CB933003), the International Science & Technology Corporation Program of China (2013DFA50840), National Natural Science Foundation of China (51272197, 51302203), Fundamental Research Funds for the Central Universities (2013-ZD-7, 2014-ZY-016, 2014-YB-002) and the Students Innovation and Entrepreneurship Training Program (20141049701008). Thanks to Professor C.M. Lieber of Harvard University and Professor Q.J. Zhang of Wuhan University of Technology for strong support and stimulating discussion. Special thanks to J. Liu of Pacific Northwest National Laboratory for his careful supervision, strong support and stimulating discussion.

Appendix A. Supporting information

Supplementary data associated with this article can be found in the online version at http://dx.doi.org/10.1016/j.nanoen.2014.06.006.

References

[1] A. Yoshino, Angew. Chem. Int. Ed. 51 (2012) 5798–5800.
[2] F.Y. Cheng, J. Liang, Z.L. Tao, J. Chen, Adv. Mater. 23 (2011) 1695–1715.
[3] N. Mahmood, C.Z. Zhang, F. Liu, J.H. Zhu, Y.L. Hou, ACS Nano 7 (2013) 10307–10318.
[4] C.Z. Zhang, N. Mahmood, H. Yin, F. Liu, Y.L. Hou, Adv. Mater. 25 (2013) 4932–4937.
[5] M. Armand, J.M. Tarascon, Nature 451 (2008) 652–657.
[6] B. Dunn, H. Kamath, J.M. Tarascon, Science 334 (2011) 928–935.
[7] Y.M. Sun, X.L. Hu, W. Luo, Y.H. Huang, ACS Nano 5 (2011) 7100–7107.
[8] H.B. Wu, J.S. Chen, H.H. Hng, X.W. Lou, Nanoscale 4 (2012) 2526–2542.
[9] J. Chen, F.Y. Cheng, Acc. Chem. Res. 42 (2009) 713–723.
[10] N. Mahmood, C.Z. Zhang, Y.L. Hou, Small 9 (2013) 1321–1328.
[11] Y.G. Wang, H.Q. Li, P. He, E. Hosono, H.S. Zhou, Nanoscale 2 (2010) 1294–1305.
[12] F.Y. Su, Y.B. He, B.H. Li, X.C. Chen, C.H. You, W. Wei, W. Lv, Q.H. Yang, F.Y. Kang, Nano Energy 1 (2012) 429–439.
[13] Y. Idota, T. Kubota, A. Matsufuji, Y. Maekawa, T. Miyasaka, Science 276 (1997) 1395–1397.

[14] J.P. Liu, Y.Y. Li, X.T. Huang, R.M. Ding, Y.Y. Hu, J. Jiang, L. Liao, J. Mater. Chem. 19 (2009) 1859–1864.
[15] P.L. Taberna, S. Mitra, P. Poizot, P. Simon, J.M. Tarascon, Nat. Mater. 5 (2006) 567–573.
[16] Y.J. Chen, J. Zhu, B.H. Qu, B.G. Lu, Z. Xu, Nano Energy 3 (2014) 88–94.
[17] S. Chen, M. Wang, J.F. Ye, J.G. Cai, Y.R. Ma, H.H. Zhou, L.M. Qi, Nano Res. 6 (2013) 243–252.
[18] C.K. Chan, H.L. Peng, G. Liu, K. McIlwrath, X.F. Zhang, R.A. Huggins, Y. Cui, Nat. Nanotechnol. 3 (2008) 31–35.
[19] J.Y. Huang, L. Zhong, C.M. Wang, J.P. Sullivan, W. Xu, L.Q. Zhang, S.X. Mao, N.S. Hudak, X.H. Liu, A. Subramanian, H.Y. Fan, L. Qi, A. Kushima, J. Li, Science 330 (2010) 1515–1520.
[20] L. Wang, D. Wang, Z.H. Dong, F.X. Zhang, J. Jin, Small 10 (2014) 998–1007.
[21] B. Hu, L.Q. Mai, W. Chen, F. Yang, ACS Nano 3 (2009) 478–482.
[22] P. Jiang, J.J. Zhou, H.F. Fang, C.Y. Wang, Z.L. Wang, S.S. Xie, Adv. Funct. Mater. 17 (2007) 1303–1310.
[23] J. Jiang, Y.Y. Li, J.P. Liu, X.T. Huang, Nanoscale 3 (2011) 45–58.
[24] N.S. Sariciftci, L. Smilowitz, A.J. Heeger, F. Wudl, Science 258 (1992) 1474–1476.
[25] W.S. Huang, B.D. Humphrey, A.G. MacDiarmid, J. Chem. Soc. Faraday Trans. 82 (1986) 2385–2400.
[26] O. Bubnova, Z.U. Khan, A. Malti, S. Braun, M. Fahlman, M. Berggren, X. Crispin, Nat. Mater. 10 (2011) 429–433.
[27] M. Gao, S.M. Huang, L.M. Dai, G. Wallace, R.P. Gao, Z.L. Wang, Angew. Chem. Int. Ed. 39 (2000) 3664–3667.
[28] L.J. Pan, G.H. Yu, D.Y. Zhai, H.R. Lee, W.T. Zhao, N. Liu, H.L. Wang, B.C.K. Tee, Y. Shi, Y. Cui, Z. Bao, Proc. Natl. Acad. Sci. 109 (2012) 9287–9292.
[29] Y. Yao, N. Liu, M.T. McDowell, M. Pasta, Y. Cui, Energy Environ. Sci. 5 (2012) 7927–7930.
[30] J.M. Jeong, B.G. Choi, S.C. Lee, K.G. Lee, S.J. Chang, Y.K. Han, Y.B. Lee, H.U. Lee, S. Kwon, G. Lee, C.S. Lee, Y.S. Huh, Adv. Mater. 25 (2013) 6250–6255.
[31] L.Q. Mai, X. Xu, C.H. Han, Y.Z. Luo, L. Xu, Y.A. Wu, Y.L. Zhao, Nano Lett. 11 (2011) 4992–4996.
[32] W.Y. Li, Q.F. Zhang, G.Y. Zheng, Z.W. Seh, H.B. Yao, Y. Cui, Nano Lett. 13 (2013) 5534–5540.
[33] Z.W. Seh, W.Y. Li, J.J. Cha, G.Y. Zheng, Y. Yang, M.T. McDowell, P.C. Hsu, Y. Cui, Nat. Commun. 3 (2012) 1331.
[34] C. Zhou, Y.W. Zhang, Y.Y. Li, J.P. Liu, Nano Lett. 13 (2013) 2078–2085.
[35] D.L. Wang, H.L. Xin, R. Hovden, H.S. Wang, Y.C. Yu, D.A. Muller, F.J. DiSalvo, H. Abruňa, Nat. Mater. 12 (2013) 81–87.
[36] L.Q. Mai, F. Dong, X. Xu, Y.Z. Luo, Q.Y. An, Y.L. Zhao, J. Pan, J.N. Yang, Nano Lett. 13 (2013) 740–745.
[37] Y.J. Chen, B.H. Qu, L.L. Hu, Z. Xu, Q.H. Li, T.H. Wang, Nanoscale 5 (2013) 9812–982.
[38] X.Y. Zhao, B. Liu, C.W. Hu, M.H. Cao, Chem. Eur. J. 20 (2014) 467–473.
[39] X.H. Xia, D.L. Chao, X.Y. Qi, Q.Q. Xiong, Y.Q. Zhang, J.P. Tu, H. Zhang, H.J. Fan, Nano Lett. 13 (2013) 4562–4568.
[40] L. Zhang, G.Q. Zhang, H.B. Wu, L. Yu, X.W. Lou, Adv. Mater. 25 (2013) 2589–2593.
[41] X.L. Wu, Y.G. Guo, J. Su, J.W. Xiong, Y.L. Zhang, L.J. Wan, Adv. Energy Mater. 3 (2013) 1155–1160.

Wangwang Xu received his B.S. degree in Department of Composite Materials from Wuhan University of Technology in 2012. He is working toward the Master degree in WUT-Harvard Joint Nano Key Laboratory. His current research involves achieving the special nanostructure to improve the performance of negative electrode materials.

Kangning Zhao received his B.S. degree in Department of Materials Science of Engineering from Wuhan University of Technology in 2012. He has joined WUT-Harvard Joint Nano Key Laboratory for two years. He is currently working toward the Ph.D. degree. His current research involves the nanomaterials achieving high energy density and power density for lithium ion battery and sodium ion battery.

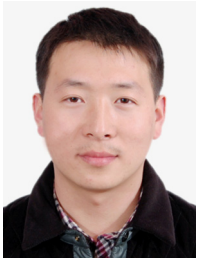

Chaojiang Niu received his M.S. degree in Material Chemistry from Wuhan University of Technology in 2009. He is currently working toward the Ph.D. degree and his current research focuses on the energy storage materials and devices.

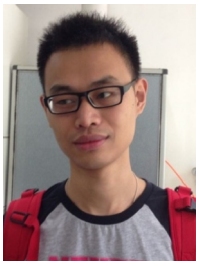

Lei Zhang received his B.S. degree in Department of Materials Science of Engineering from Wuhan University of Technology in 2012. He has joined WUT-Harvard Joint Nano Key Laboratory for two years. His current research involves vanadate as anode and cathode for lithium ion battery and supercapacitor.

Zhengyang Cai received his first B.S. degree in Department of Materials Chemistry from Wuhan University of Technology in 2012, and his second degree in Department of Computer Science and Technology from Huazhong University of Science and Technology. He has joined WUT-Harvard Joint Nano Key Laboratory for two years. His current research involves achieving the special nanostructure asnegative electrode materials for lithium battery.

Chunhua Han received her M.S. degree in material science from Wuhan University of Technology in China in 2006, and she has completed her doctoral dissertation and will gain a doctor's degree in May 2013. Her current research involves nanoenergy materials and devices.

Liang He is an assistant professor of the State Key Laboratory of Advanced Technology for Materials Synthesis and Processing at Wuhan University of Technology. He received his Ph.D. from Tohoku University (Japan) in 2013. His current research interests include the microfabrication and characterization of micro/nano structures and devices for use in MEMS (Micro Electro Mechanical Systems).

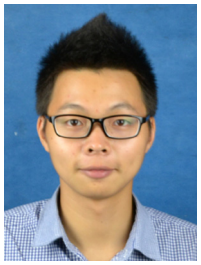

TengShen is a junior in Department of Materials Molding at the Wuhan University of Technology (WHUT). He has joined WUT-Harvard Joint Nano Key Laboratory for one year, and his current research involves high energy density energy storage devices.

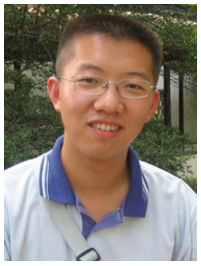

Mengyu Yan received his B.S. degree in Material Chemistry from China University of Geosciences in 2012 and he is currently working toward the Ph.D. degree in Material Science at Wuhan University of Technology. His current research interests include nanoenergy materials and devices.

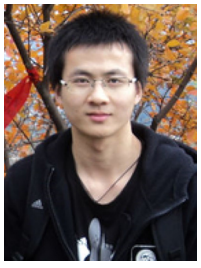

Longbing Qu received his B.S. degree in Materials Science and Engineering from Wuhan University of Technology in 2011. He is currently working toward the Master degree. His current research interests include nanomaterials for Li-ions batteries, supercapacitors.

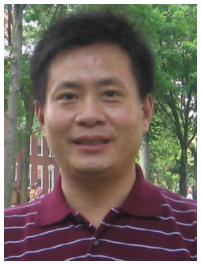

Liqiang Mai is Chair Professor of Materials Science and Engineering at Wuhan University of Technology and Executive Director of WUT-Harvard Joint Nano Key Laboratory. He received his Ph.D. from Wuhan University of Technology in 2004. He carried out his postdoctoral research in the laboratory of Prof. Zhonglin Wang at Georgia Institute of Technology in 2006–2007 and worked as advanced research scholar in the laboratory of Prof. Charles M. Lieber at Harvard University in 2008–2011. His current research interests focus on nanowire materials and devices for energy storage.